arXiv:1504.00153v1 [physics.atm-clus] 1 Apr 2015

RESEARCH ARTICLE

Dynamics and thermodynamics of decay in charged clusters

Mark A. Miller[a*], David A. Bonhommeau[b], Christian P. Moerland[c], Sarah J. Gray[a] and
Marie-Pierre Gaigeot[d]

[a]*Department of Chemistry, Durham University, South Road, Durham, UK*
[b]*GSMA CNRS UMR7331, Université de Reims Champagne-Ardenne, UFR Sciences
Exactes et Naturelles, Moulin de la Housse, BP 1039, F-51687 Reims Cedex 2, France*
[c]*Department of Applied Physics, Technische Universiteit Eindhoven,
Postbus 513, 5600 MB Eindhoven, The Netherlands*
[d]*Université d'Evry val d'Essonne, LAMBE CNRS UMR8587, Boulevard F Mitterrand,
Bâtiment Maupertuis, F-91025 Evry, France*

We propose a method for quantifying charge-driven instabilities in clusters, based on equilibrium simulations under confinement at constant external pressure. This approach makes no assumptions about the mode of decay and allows different clusters to be compared on an equal footing. A comprehensive survey of stability in model clusters of 309 Lennard-Jones particles augmented with Coulomb interactions is presented. We proceed to examine dynamic signatures of instability, finding that rate constants for ejection of charged particles increase smoothly as a function of total charge with no sudden changes. For clusters where many particles carry charge, ejection of individual charges competes with a fission process that leads to more symmetric division of the cluster into large fragments. The rate constants for fission depend much more sensitively on total charge than those for ejection of individual particles.

Keywords: charged clusters; instability; simulation; Lennard-Jones; Rayleigh limit

1. Introduction

When a droplet or cluster carries a sufficiently high net electrostatic charge, the charge drives decay into two or more fragments. The first analysis of this phenomenon, due to Rayleigh [1] is now well over a century old, but the resulting prediction for the critical charge at which decay occurs retains its central importance in modern research in the area. Rayleigh's analysis is based on a uniformly charged, structureless sphere of diameter D that may undergo shape fluctuations, leading simultaneously to an increase in surface energy and a decrease in electrostatic energy. Deformation leads to a barrierless decrease in the sum of these energies beyond the limiting charge $Q_R = \pi\sqrt{8\epsilon_0\gamma D^3}$, where γ is the surface tension of the droplet interface and ϵ_0 is the permittivity of free space. Rayleigh reached this classic result within the first page of his elegantly short article [1], concealing a somewhat involved derivation [2].

Since Rayleigh's time, his work has gained new significance due to the importance of charged droplets in contemporary fields such as atmospheric chemistry [3]

*Corresponding author. Email: m.a.miller@durham.ac.uk

and electrospray ionisation mass spectrometry [4]. Nevertheless, it has been recognised that unstable global deformations are not the only mechanism by which a charged droplet may decay. For example, the ion evaporation model [5] provides a continuum-based understanding of how small ions may be ejected from a droplet even below the Rayleigh limit. When macroions are dissolved in a droplet, other mechanisms come into play. Evaporation of the droplet may lead to some of the charge being deposited on the solute [6]. Unravelling of polymeric solutes in water can lead to more complex processes [7, 8], including the extrusion of a solvent-free segment of the chain or the formation of subdroplets along extended chain conformations [9].

In principle, a cluster at finite temperature in an unbounded environment is thermodynamically at most metastable, even if it is charge-neutral, since unlimited translational entropy can be gained by dividing the cluster into fragments. Hence, the concept of stability implicitly involves a sense of time scale, such as the typical time of flight of an electrosprayed droplet in a mass spectrometer. In a previous paper, some of us devised an equilibrium approach to identifying charge-driven instability in small clusters [10] based on confining the cluster to a spherical container and monitoring the fraction of equilibrium configurations in which the cluster had emitted at least some of its charged particles. In the present article, we propose a different equilibrium-based approach that provides some significant advantages in terms of the generality of its applicability and the physical basis of its interpretation. We then proceed to a quantitative characterisation of the dynamics of charge-driven instabilities in a simple model, focusing on the competition between ejection and fission processes.

2. Model

As in our previous study [10], we use a Lennard-Jones (LJ) cluster of $N = 309$ particles to explore methods of characterisation. For simplicity, all particles interact with the same LJ well-depth u and length parameter σ. In addition, particles may carry a charge, introducing a Coulomb term to the total potential energy:

$$E = 4u \sum_{i<j}^{N} \left[\left(\frac{\sigma}{r_{ij}} \right)^{12} - \left(\frac{\sigma}{r_{ij}} \right)^{6} \right] + \sum_{i<j}^{N} \frac{q_i q_j}{4\pi\epsilon_0 r_{ij}},$$

where q_i is the charge on particle i and r_{ij} is the distance between particles i and j. We adopt the usual LJ reduced energy $E^* = E/u$, length $r^* = r/\sigma$ and temperature $T^* = k_{\mathrm{B}}T/u$, where k_{B} is Boltzmann's constant. We also define a dimensionless charge $q^* = q_i/\sqrt{4\pi\epsilon_0\sigma u}$. In terms of reduced variables, therefore,

$$E^* = \sum_{i<j}^{N} \left[4(r_{ij}^{*\,-12} - r_{ij}^{*\,-6}) + q_i^* q_j^* / r_{ij}^* \right].$$

Since the reduced charge q^* depends on u and σ in addition to q, it is not confined to integer multiples of the electronic charge. To enable us to examine properties of the model charged cluster systematically as a function of charge, we will treat the reduced charge as a continuous variable. However, we will restrict ourselves to the case where n of the N particles carry identical single-particle charges, $q_i^* = q^*$, while the remaining $N - n$ particles are neutral, with $q_i^* = 0$. The total reduced charge on the cluster is then $Q^* = nq^*$.

$N = 309$ is a magic number for the LJ potential, corresponding to four complete icosahedral shells in the lowest-energy structure [11]. The neutral cluster's thermodynamics has been studied in detail [12], allowing us to select a reduced temperature of $T^* = 0.43$, which lies just above the broadened melting transition, for most of our calculations. In this liquid-like regime, the highly ordered global potential minimum structure is not seen. As might be expected, the addition of charge lowers the cluster's melting temperature [13].

The LJ potential with charges localised on individual particles is clearly a highly idealised model. It does not incorporate the complexity associated with hydrogen bonding in water clusters or mechanisms for transferring excess charge to the cluster surface by orientation of dipole moments [14]. We note that it is possible to refine the model by the inclusion of polarisability, with induced dipoles solved self-consistently [13], though this is a costly addition to a simple model. Nevertheless, idealised models of this type do provide scope for probing different mechanisms of decay [15, 16], and can even provide a useful reference for quantitative analysis of experimental data on the evaporation of real charged droplets [17].

3.   Droplets at equilibrium

As pointed out in the introduction, an unbounded cluster decays over time even if it is uncharged. Clusters bound by van der Waals-like interactions such as the LJ potential gradually evaporate, typically one particle at a time. Hence, the equilibrium thermodynamics of clusters must always be characterised within a container. A spherical enclosure is usually used, and an appropriate radius must then be chosen by some criterion [18, 19]. In our previous article [10], we used a container radius of $R_c = 6.5\sigma$ for the 309-atom LJ cluster, with the centre of the container tracking the centre-of-mass of the cluster [18]. This choice of R_c allows a clear separation between any particles that have been decisively ejected and the remaining subcluster. However, the equilibrium between evaporated and condensed particles is influenced by the choice of radius [19] and so the arbitrary choice of R_c is an unattractive feature of the approach. It is also difficult to compare clusters of different size N, since it is not entirely clear how R_c should change with N for a truly unbiased comparison.

In the present work, we take a different approach that offers a number of advantages. We place the cluster in a fluctuating container whose volume changes in response to the cluster inside it and to a fixed external pressure p. This pressure may be set at a physically meaningful value by reference to, for example, the background medium or carrier gas in a particular application. The same value of p may straightforwardly be used for different N if a comparison between cluster sizes is required.

The isobaric, isothermal approach that we propose is slightly different from typical constant-NpT Monte Carlo simulations, which are normally encountered when modelling bulk systems as represented by a periodic simulation cell. In a periodic system, stochastic changes in the cell volume are accompanied by a uniform scaling of all particle positions in order to respect the boundary conditions in the resized cell, and particle displacement steps are made in coordinates that have been scaled to lie in a unit cube. This protocol leads to a Monte Carlo acceptance criterion for trial volume changes of [20]

$$P^{\text{acc}} = \min\left[1, \ \exp\left(-\frac{(E' - E)}{k_{\text{B}}T}\right)\exp\left(-\frac{p(V' - V)}{k_{\text{B}}T}\right)\left(\frac{V'}{V}\right)^N\right],$$
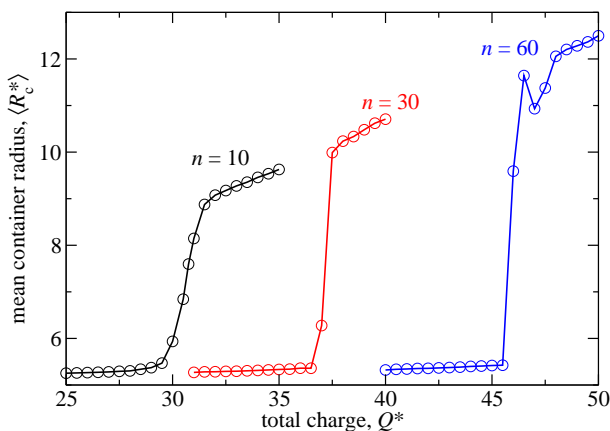
Figure 1. Detection of decay using the fluctuating-container method at reduced pressure $p^* = 0.005$ for reduced total charge Q^* distributed amongst three different numbers n of charge-carriers. Instability appears as a sharp increase in the reduced mean container radius.

where V is the volume of the cell and primes indicate new values after the trial move. The factor containing E is due to the energy change associated with scaling the particle coordinates, while the factor $(V'/V)^N$ comes from the change of variables to scaled coordinates in a unit cell. However, our cluster is not a periodic system, and it is more efficient to allow the container to fluctuate without unnaturally expanding or contracting the cluster by a scaling of the particle coordinates. If the configuration is left unchanged during trial volume changes then the acceptance for trial volume changes is the simpler

$$P^{\mathrm{acc}} = \min\left[1,\ \exp\left(-\frac{p(V'-V)}{k_{\mathrm{B}}T}\right)\prod_{i=1}^{N}\Theta(R'_{\mathrm{c}} - |\mathbf{r}'_i|)\right],$$

where $\mathbf{r}'_i$ is the position of particle i relative to the centre of mass (after the trial move). The product of Heaviside step functions Θ enforces the requirement that all particles lie within the container. Hence, any trial decrease in volume that would result in the exclusion of an outlying particle must be rejected. In effect, such a proposed state would have infinite energy because the container is hard. Trial volume changes constitute 1% of Monte Carlo steps in our simulations.

In addition to the modified volume-change steps, 20% of Monte Carlo steps in our simulation are devoted to attempted exchanges between neutral and charged particles, leaving their positions fixed. These swaps are accepted according to the standard Metropolis criterion [20, 21] and make exploration of the equilibrium configurations more efficient [10].

Figure 1 shows the mean reduced container radius $\langle R_{\mathrm{c}}^* \rangle$ as a function of total charge Q^* at a reduced pressure of $p^* = p\sigma^3/u = 0.005$. (For reference, with argon LJ parameters, 1 bar corresponds to $p^* \approx 0.0024$.) Each point in the figure was obtained from a simulation of 2×10^7 Monte Carlo steps per particle. A sharp increase in $\langle R_{\mathrm{c}}^* \rangle$ occurs at a particular charge, indicating that the fragmentation of the cluster is sufficient to force the container outwards against the external pressure. From a thermodynamic point of view, the sudden change is akin to the finite-system analogue of a first-order liquid–gas phase transition, but here driven by charge rather than by temperature. The value of Q^* at which the jump occurs increases with the number of particles n over which the charge is divided, reinforcing our earlier result that the maximum charge a cluster can sustain is generally larger when the charge is divided over more particles [10].
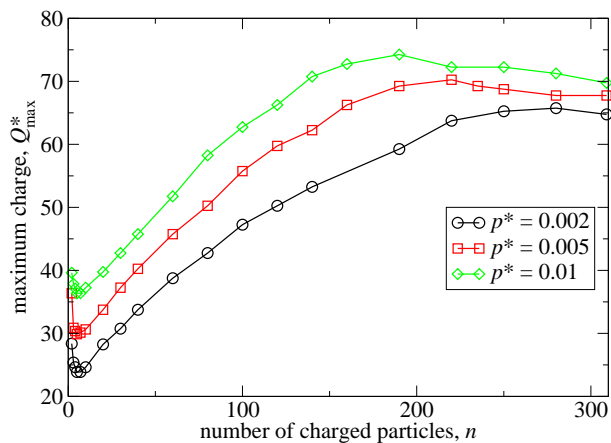
Figure 2.   Maximum charge as detected by the fluctuating-container method at three reduced pressures p^*.

We take the point at which the numerical derivative dR_c^*/dQ^* is largest to be the maximum charge $Q_{\max}^*$ that the cluster can sustain. This transition is more sharply defined than the point at which dissociated configurations become a majority in a container of fixed radius [10]. $Q_{\max}^*$ based on the fluctuating-container method is plotted as a function of n in Fig. 2, showing qualitatively similar behaviour at three different pressures. At large n, $Q_{\max}^*$ shows a small but systematic decrease. As will be explored in the next section, this feature corresponds to the onset of competition between ejection of individual charged particles and fission of the cluster into larger fragments. The fact that the fluctuating container detects both these modes of decay using the same procedure and without prior knowledge of the change in mechanism is one of the method's appealing features. Even in the more complex cases of droplets of polar molecules with or without a polymeric solute, the decay pathways all involve spreading out of the charged particles by a decisive deviation of the droplet away from a spherical or near-spherical shape [7, 8]. Such changes would always lead to a sudden increase in the radius of the container at some critical charge. Hence, the fluctuating-container method should be quite generally applicable to the problem of detecting and defining charge-driven instability.

At very small n, Fig. (2) shows that there is a shallow minimum in $Q_{\max}^*$. This feature seems to be related to the rapid increase in energy with respect to the number of charges at small n. In the hypothetical case where the charged particles lay neatly at the surface of a perfectly spherical cluster, the cluster would be described by the so-called Thomson problem [22], which poses the question of the optimal arrangement and corresponding energy of n unit charges on the surface of a unit sphere. In the continuum limit, a sphere with a uniformly charged surface has an electrostatic energy that scales as the square of the surface charge density. The global potential energy minima of the Thomson problem do approach a constant ratio of energy to n^2 at large n [23]. However, for small n, the energy rises considerably more steeply than n^2 [24].

4.   Dynamics of decay

We now turn to dynamic signatures of charge-driven instability. The clusters must be prepared in a well defined intact state before being allowed to decay. Our protocol is to equilibrate the cluster using constant-temperature Monte Carlo simulations in a tight-fitting spherical container of fixed radius 5.2488σ, which is the maximum
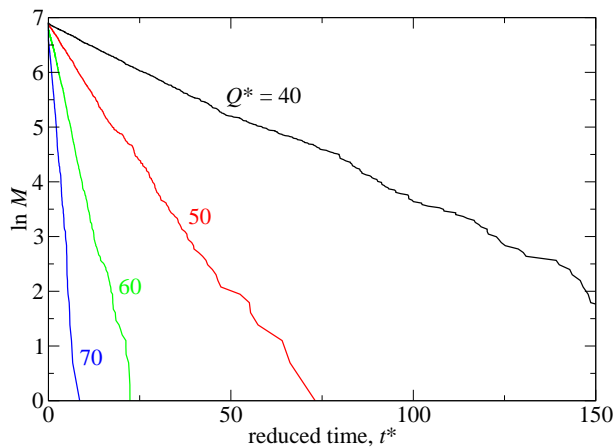
Figure 3.   First-order decay plots for first ejection of a charged particle averaged over an ensemble of 1000 clusters carrying $n = 100$ charges at four values of the initial total charge Q^*. M is the number of intact clusters remaining at time t^*.

radius of the icosahedral global minimum structure [11] plus a margin of σ. The container is then removed and random Maxwell–Boltzmann-distributed velocities are assigned to the atoms. From this point, the cluster is allowed to evolve via constant-energy molecular dynamics (MD) with a standard Verlet integrator [20] and a time-step of $\delta t^* = 0.002$, where the LJ reduced time is $t^* = t\sqrt{u/m\sigma^2}$ and m is the mass of one particle.

To detect evaporation and ejection events, we monitor the distance of all particles from the centre of mass. When a particle reaches a large distance (22σ) from the remaining subcluster, we can be confident that it will not return. The actual time of the evaporation or ejection is then backdated to the MD step at which the velocity of the particle first started on its outward trajectory, $i.e.$, the earliest time t_{e}^* such that $\mathbf{v}_i(t^*) \cdot \mathbf{r}_i(t^*) > 0$ for all $t^* \geq t_{\mathrm{e}}^*$, where $\mathbf{v}_i$ is the velocity of particle i. This procedure allows temporary excursions of particles to be ignored while still providing an accurate timestamp for ejection events.

We have measured the time of first ejection of a charged particle in an ensemble of 1000 independent trajectories. From the list of ejection times, we may construct a first-order kinetics plot of the logarithm of the number M of clusters that have not yet decayed as a function of time. Results for a selection of ensembles with $n = 100$ charged particles and different initial total charges are shown in Fig. 3, confirming that ejection of the first charge is a first-order process. From the slopes, we obtain reduced rate constants k^*, which are plotted (circles) as a function of initial charge in Fig. 4.

The total charge spanned in Fig. 4 starts well below and finishes considerably above the range of Q_{max}^* measured in our equilibrium simulations (Fig. 2) for $n = 100$. The rate constant increases smoothly with Q^*, never showing a decisive jump that could be taken as a dynamically-defined threshold for instability.

We may also extract an effective activation energy E_{a}^* for ejection from Arrhenius plots of $\ln k^*$ against inverse temperature. Remembering the proximity of our chosen temperature $T^* = 0.43$ to the melting transition of the neutral cluster [12] on the one hand, and the rapidly increasing tendency for thermal evaporation at higher temperatures [19] on the other, we have varied $1/T^*$ over only a narrow range. Arrhenius behaviour is nevertheless clearly evident, as shown in the inset of Fig. 5, allowing the activation energy to be plotted as a function of total charge in the main panel of the figure. In keeping with the smoothly changing rate constants of Fig. 4, the activation energy shows no sudden changes with charge and appears
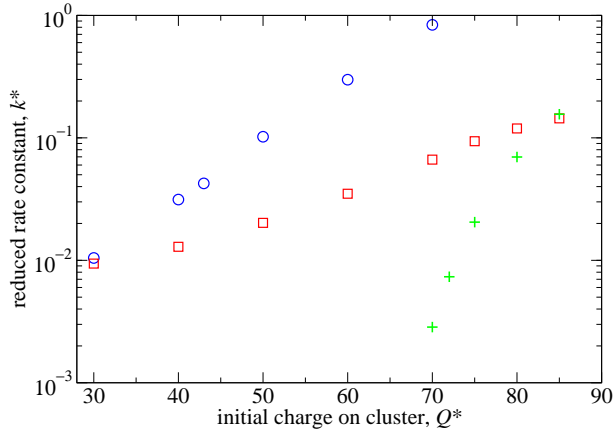
Figure 4. Rate constants for the ejection of the first particle for a cluster carrying $n = 100$ charged particles (blue circles) and $n = 309$ charged particles (red squares), and rate constants for fission of the $n = 309$ cluster (green plusses).
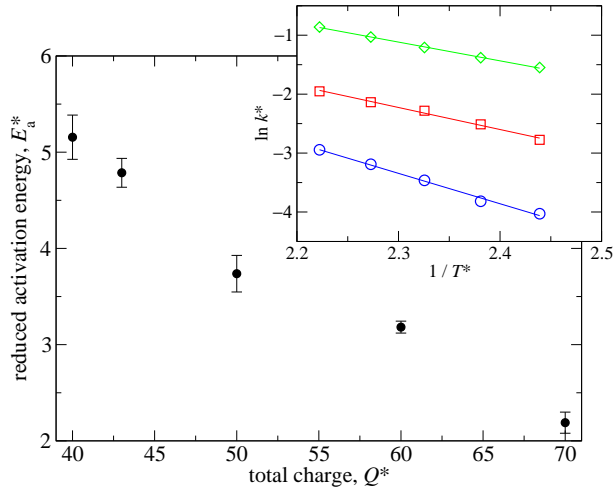

Figure 5. Activation energy E_a^* for particle ejection for a cluster carrying $n = 100$ charges. Bars show the standard error in the linear regression coefficient. The inset shows example Arrhenius plots whose slopes are $-E_\mathrm{a}^*$: $Q^* = 40$ (blue circles), $Q^* = 50$ (red squares), $Q^* = 60$ (green diamonds).

to depend rather linearly on charge in this case.

In highly charged clusters, the ejection of a charged particle can lower the overall potential energy of the remaining subcluster and, depending on the kinetic energy carried away, can in turn lead to slight increase in the effective temperature of the subcluster. However, we have not observed any "run-away" cascades where the rate of decay of an ensemble increased with successive ejection events.

The same observation of smoothly changing first-ejection rates at $n = 100$ applies to the case of $n = 309$ (squares in Fig. 4), where the charge is spread over all the particles in the cluster. As might be predicted from the higher value of Q_max^* at large n (Fig. 2), the rate constant is lower than for the $n = 100$ case at a given total charge, despite the fact that there are more charged particles that could be ejected at $n = 309$.

The crucial difference between $n = 100$ and $n = 309$ is that ejection of individual charged particles is not the only mechanism of decay for the latter. At large n, clusters may also undergo a more symmetric fission process, in which two large fragments are produced. Snapshots of ejection and fission processes are shown in Fig. 6. Fission may be detected by performing a cluster analysis based on a pairwise particle connectivity criterion of 1.5σ and defining fission to have taken place at
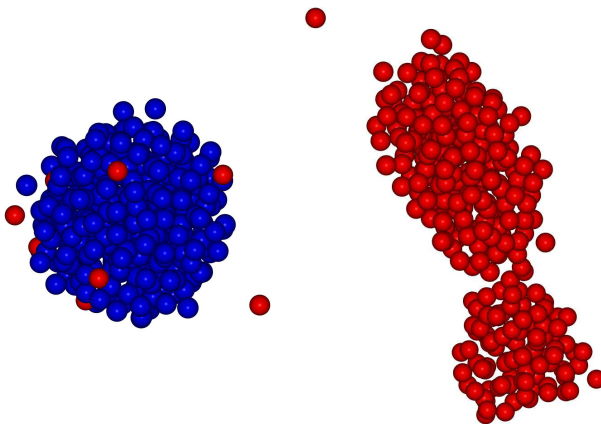
Figure 6.   Left: ejection of a particle from a cluster carrying $n = 10$ charges (red spheres), total charge $Q^* = 24$. Right: fission of a cluster of $n = 309$ charges, $Q^* = 67$, into two sub-clusters.

the first time at which two separate clusters, each of at least $N/4$ particles, exist. (The results are insensitive to the arbitrary choices of connectivity criterion and subcluster size.) Since the clusters are equilibrated in a tightly-fitting spherical container, the elongation fluctuations that lead to fission take some time to be established before fission itself can take place. Hence, an ensemble of clusters shows a lag before the onset of a first-order decay law. Ejection of individual charges may take place throughout the lag, division and separation of the subclusters.

Rate constants for the fission process, derived from the post-lag section of the ensemble's decay, are shown (plus-symbols) in Fig. 4. The rate constant for fission increases much more rapidly with charge than the constant for ejection of individual charges, and the rate becomes negligible at lower total charges where ejection is still taking place much faster than neutral evaporation. Despite the rapid promotion of fission, it is difficult to pinpoint a threshold for instability purely on the basis of dynamics, since the rates change smoothly up to the point where decay by ejection or fission immediately follows the removal of the equilibration container.

The competition between ejection and fission for $n = 309$ and the absence of fission at smaller n can be understood from an idealised analysis by Consta and Malevanets of a spherical droplet splitting into two daughter droplets with conservation of total volume and of total charge [2]. Symmetrical decay (fission) is favoured when electrostatic energy dominates over surface energy, since the decrease in electrostatic energy of separating two highly charged subclusters compensates for the large increase in surface area caused by creating two spheres from one with the same total volume. This is the regime in our clusters at large n. In contrast, when n is small, a fractionally significant decrease in electrostatic energy can be achieved by the ejection of a single charged particle without incurring a large increase in surface energy.

Our procedure for determining the decay rate constants for ejection and fission relies on being able to separate trajectories cleanly into portions corresponding to reactants (intact clusters) and products (separated particles or fragments). The methods of backdating outbound ejected particles and monitoring the connectivity of subclusters in fission amount to selecting reactant–product dividing surfaces in phase space. Our choices of surface are not unique but have the advantages of being straightforward to evaluate and, crucially, not being prone to recrossing by trajectories. Hence, crossings can be interpreted decisively as decay events. In droplets of polar molecules, where decay may occur via departure of a small cluster [25], it should be possible to adapt the fission criterion to detect division of the droplet into uneven fragments simply by adjusting the threshold in the number of

particles at which a detached fragment is defined.

To gain more detailed insight into the fluctuations leading to decay is a more difficult goal that requires construction of a reaction coordinate capable of faithfully describing the ensemble of decay pathways. The task has been approached by Consta and coworkers [25, 26] for the case of water droplets containing simple ions. Such clusters develop a bottleneck as the ions start to separate prior to decay of the droplet, even when decay is uneven with respect to fragment size. A special transfer reaction coordinate was introduced to identify the resulting dumbbell-shaped configurations, as distinct from more general prolate distortions. This approach allowed differences to be observed in the diffusive nature of trajectories near the top of the free energy barrier for clusters containing different ions [26]. As in any activated process, the height and shape of the free energy barrier for a given process and system depend on the choice of reaction coordinate, but the overall rate constant should not, provided that a converged transmission coefficient can be obtained.

5.   Concluding remarks

Our fluctuating-container simulations effectively cast charge-driven instability as a transition under well defined equilibrium thermodynamic conditions. This approach has the advantages of not requiring any assumptions about the mechanism of the instability, of permitting comparisons between different clusters if required, and of being quite sharply defined even for small clusters (where temperature-driven transitions are normally broadened). The method is also oblivious to any transient evaporation of neutral fragments that are of no interest in the context. The only parameter that must be fixed is the imposed pressure, but this quantity does have a direct physical interpretation.

It is not straightforward to compare our results for the stability of the 309-atom LJ cluster with the prediction of Rayleigh's classic formula, not least because the surface tension is not known. Clusters in this size range have a dramatically depressed melting temperature in comparison with the bulk, and the liquid-like regime that we have studied around $T^* = 0.43$ is well below the triple point of bulk Lennard-Jones, which lies at about $T^* = 0.69$ [27, 28]. Below this point, no bulk equilibrium value of γ exists.

The first mode of deformation to become unstable in Rayleigh's model is the second-rank spherical harmonic, corresponding to oblate–prolate deviations from the sphere. Although Rayleigh's work makes no formal prediction about the mechanism or products that result from the instability, we note that a prolate deformation much more closely resembles the motion that precedes the fission mechanism that we observe in the LJ cluster at large number n of charges. Nevertheless, even where single-particle ejection dominates the decay and fission is absent, the clusters are typically distorted in a prolate direction.

For simplicity, we have given all particles in our cluster the same LJ energy and length parameters. However, if charged particles interacted with stronger well depth u or had a larger diameter σ, one could envisage emission of "solvated" charges rather than bare particles. Clearly, a number of other refinements could be included to make the model a more realistic depiction of a particular system. However, the idealised model has allowed a systematic survey of charge limits, the decay of large ensembles, rate constants, and activation barriers to be performed. The methods deployed here should be useful in future investigations of other charged clusters and droplets.

Acknowledgements

References

[1] Lord Rayleigh, Philos. Mag. **14**, 184 (1882).

[2] S. Consta and A. Malevanets, Mol. Simul. **41**, 73 (2015).

[3] A. Hirsikko, T. Nieminen, S. Gangné, K. Lehtipalo, H.E. Manninen, M. Ehn, U. Hõrrak, V.M. Kerminen, L. Laakso, P.H. McMurry, A. Mirme, T. Petäjä, H. Tammet, V. Vakkari, M. Vana and M. Kulmala, Atmos. Chem. Phys. **11**, 767 (2011).

[4] J.B. Fenn, Angew. Chem. Int. Ed. **42**, 3871 (2003).

[5] J.V. Iribarne and B.A. Thomson, J. Chem. Phys. **64**, 2287 (1976).

[6] M. Dole, L.L. Mack, R.L. Hines, R.C. Mobley, L.D. Ferguson and M.B. Alice, J. Chem. Phys. **49**, 2240 (1968).

[7] S. Consta, J. Phys. Chem. B **114**, 5263 (2010).

[8] E. Ahadi and L. Konermann, J. Phys. Chem. B **116**, 104 (2012).

[9] S. Consta and A. Malevanets, J. Chem. Phys. **138**, 044314 (2013).

[10] M.A. Miller, D.A. Bonhommeau, C.J. Heard, Y. Shin, R. Spezia and M.P. Gaigeot, J. Phys. Cond. Mat. **24**, 284130 (2012).

[11] D. Romero, C. Barrón and S. Gómez, Comp. Phys. Comm. **123**, 87 (1999).

[12] E.G. Noya and J.P.K. Doye, J. Chem. Phys. **124**, 104503 (2006).

[13] D.A. Bonhommeau and M.P. Gaigeot, Comp. Phys. Comm. **184**, 873 (2013).

[14] R. Vácha, S.W. Rick, P. Jungwirth, A.G.F. de Beer, H.B. de Aguiar, J.S. Samson and S. Roke, J. Am. Chem. Soc. **133**, 10204 (2011).

[15] I. Last, Y. Levy and J. Jortner, Proc. Natl. Acad. Sci. USA **99**, 9107 (2002).

[16] Y. Levy, I. Last and J. Jortner, Mol. Phys. **104**, 1227 (2006).

[17] R. Hołyst, M. Litniewski, D. Jakubczyk, M. Zientara and M. Woźniak, Soft Matter **9**, 7766 (2013).

[18] J.K. Lee, J.A. Barker and F.F. Abraham, J. Chem. Phys. **58**, 3166 (1973).

[19] C.J. Tsai and K.D. Jordan, J. Chem. Phys. **99**, 6957 (1993).

[20] D. Frenkel and B. Smit, *Understanding Molecular Simulation*, 2nd ed. (Academic Press, San Diego, 2002).

[21] N. Metropolis, A.W. Rosenbluth, M.N. Rosenbluth, A.H. Teller and E. Teller, J. Chem. Phys. **21**, 1087 (1953).

[22] J.J. Thomson, Philos. Mag. Ser. VI **39**, 237 (1904).

[23] D.J. Wales and S. Ulker, Phys. Rev. B **74**, 212101 (2006).

[24] H.A. Munera, Nature **320**, 597 (1986).

[25] S. Consta, J. Mol. Struct. (Theochem.) **591**, 131 (2002).

[26] S. Consta, K.R. Mainer and W. Novak, J. Chem. Phys. **119**, 10125 (2003).

[27] E.A. Mastny and J.J. de Pablo, J. Chem. Phys. **127**, 104504 (2007).

[28] J.P. Hansen and L. Verlet, Phys. Rev. **184**, 151 (1969).